

Galaxy And Mass Assembly (GAMA): the effect of galaxy group environment on active galactic nuclei

Yjan A. Gordon,^{1*} Kevin A. Pimbblet,¹ Matt S. Owers,^{2,3} Joss Bland-Hawthorn,⁴ Sarah Brough,⁵ Michael J. I. Brown,⁶ Michelle E. Cluver,⁷ Scott M. Croom,⁴ Benne W. Holwerda,^{8,9} Jonathan Loveday,¹⁰ Smriti Mahajan¹¹ and Lingyu Wang^{12,13}

¹*E. A. Milne Centre for Astrophysics, University of Hull, Cottingham Road, Kingston-upon-Hull HU6 7RX, UK*

²*Department of Physics and Astronomy, Macquarie University, NSW 2109, Australia*

³*Australian Astronomical Observatory, 105 Dehli Road, North Ryde, NSW 2113, Australia*

⁴*Sydney Institute for Astronomy (SIfA), School of Physics, The University of Sydney, NSW2006, Australia*

⁵*School of Physics, University of New South Wales, NSW2052, Australia*

⁶*School of Physics and Astronomy, Monash University, Clayton, Victoria 3800, Australia*

⁷*Department of Physics and Astronomy, University of the Western Cape, Robert Sobukwe Road, Bellville 7535, South Africa*

⁸*Department of Physics and Astronomy, University of Louisville, Louisville, KY 40292, USA*

⁹*University of Leiden, Sterrenwacht Leiden, Niels Bohrweg 2, NL-2333 CA Leiden, the Netherlands*

¹⁰*Astronomy Centre, University of Sussex, Falmer, Brighton BN1 9QH, UK*

¹¹*Indian Institute of Science Education and Research Mohali (IISERM), Knowledge City, Sector 81, SAS Nagar, Manauli PO 140306, India*

¹²*SRON Netherlands Institute for Space Research, Landleven 12, NL-9747 AD Groningen, the Netherlands*

¹³*Kapteyn Astronomical Institute, University of Groningen, Postbus 800, NL-9700 AV Groningen, the Netherlands*

Accepted 2018 January 10. Received 2018 January 3; in original form 2017 December 8

ABSTRACT

In galaxy clusters, efficiently accreting active galactic nuclei (AGNs) are preferentially located in the infall regions of the cluster projected phase-space, and are rarely found in the cluster core. This has been attributed to both an increase in triggering opportunities for infalling galaxies, and a reduction of those mechanisms in the hot, virialized, cluster core. Exploiting the depth and completeness (98 per cent at $r < 19.8$ mag) of the Galaxy And Mass Assembly survey (GAMA), we probe down the group halo mass function to assess whether AGNs are found in the same regions in groups as they are in clusters. We select 451 optical AGNs from 7498 galaxies with $\log_{10}(M_*/M_\odot) > 9.9$ in 695 groups with $11.53 \leq \log_{10}(M_{200}/M_\odot) \leq 14.56$ at $z < 0.15$. By analysing the projected phase-space positions of these galaxies, we demonstrate that when split both radially, and into physically derived infalling and core populations, AGN position within group projected phase-space is dependent on halo mass. For groups with $\log_{10}(M_{200}/M_\odot) > 13.5$, AGNs are preferentially found in the infalling galaxy population with 3.6σ confidence. At lower halo masses, we observe no difference in AGN fraction between core and infalling galaxies. These observations support a model where a reduced number of low-speed interactions, ram pressure stripping and intra-group/cluster medium temperature, the dominance of which increase with halo mass, work to inhibit AGN in the cores of groups and clusters with $\log_{10}(M_{200}/M_\odot) > 13.5$, but do not significantly affect nuclear activity in cores of less massive structures.

Key words: galaxies: active – galaxies: clusters: general – galaxies: groups: general – galaxies: interactions – galaxies: nuclei.

1 INTRODUCTION

Active galactic nuclei (AGNs) are powered by the active accretion of matter on to the central super-massive black hole (SMBH) of a galaxy. Consequently, AGN may be triggered by mechanisms that

introduce a new supply of cold gas, i.e. mergers (Sanders et al. 1988; Krongold, Dultzin-Hacyan & Marziani 2002), that can then act as a fuel supply for nuclear activity. Alternatively, physical mechanisms that have the potential to destabilise the cold gas reservoirs already within a galaxy, such as harassment (Moore et al. 1996) or ram pressure stripping (RPS, Poggianti et al. 2017; Marshall et al. 2018), may trigger an infall of this gas towards the nucleus, where it can then be accreted by the SMBH.

* E-mail: y.gordon@2014.hull.ac.uk

Determining if these mechanisms actually do trigger AGN can be achieved by environmental analysis of the AGN host galaxies. The incidence of AGN has been shown to be enhanced in galaxies in very close pairs, and thus likely in the process of merging, relative to those galaxies not in a pair (Alonso et al. 2007; Woods & Geller 2007; Ellison et al. 2011). Galaxy harassment and RPS occur within the denser environment of galaxy clusters. Here, the infall of a galaxy towards the bottom of the gravitational potential well can both increase the number of high velocity close encounters a galaxy has (Moore et al. 1996), and subject the galaxy to the pressure of intra-cluster medium (ICM).

In the cluster environment at low-intermediate redshift, studies have shown that efficiently accreting AGN, i.e. not the radio-mode dominated AGN with intrinsically lower accretion rates (Hardcastle, Evans & Croston 2007; Best & Heckman 2012), preferentially inhabit regions of cluster projected phase-space associated with the infalling population (e.g. Ruderman & Ebeling 2005; Haines et al. 2012; Ehlert et al. 2013; Pentericci et al. 2013; Pimblet et al. 2013). That is to say AGNs are found amongst the cluster population experiencing harassment and RPS for the first time (Mahajan, Raychaudhury & Pimblet 2012).

In contrast to the infall region, the cluster cores have generally been observed to be relatively barren of AGN (Gilmour et al. 2007; Gavazzi, Savorgnan & Fumagalli 2011; Pimblet & Jensen 2012, cf. Ruderman & Ebeling 2005). That is not to say that AGNs are not found at all in cluster cores, indeed a small fraction of brightest cluster galaxies are known to harbour AGN (e.g. Best et al. 2007; Fraser-McKelvie, Brown & Pimblet 2014; Green et al. 2016), but that they are relatively rare in comparison to the infall regions of the structure. This dearth of AGN in cluster cores may be the result of nuclear activity having run its course during the time it takes for the galaxy to fall into the cluster centre. Alternatively, it may be the case that the environment of the cluster core is unfavourable to AGN. The cores of relaxed massive clusters have had time to virialize, and consequently the galaxy interactions in this region are high speed in nature and less conducive to galaxy mergers. The resultant lack of low-speed galaxy–galaxy interactions (Ostriker 1980) may prevent AGN from being triggered in this region. Furthermore, the ram pressure experienced by galaxies close to the cluster centre may be too high to trigger an AGN (Marshall et al. 2018), instead stripping the galaxy of its gas. This may present observationally as one-sided tails (e.g. Kenney, van Gorkom & Vollmer 2004; Fumagalli et al. 2014) or ‘jellyfish’ galaxies should star formation occur in those tails (e.g. Owers et al. 2012; Ebeling, Stephenson & Edge 2014). Such stripping would eventually starve an AGN of a potential fuel supply. A further mechanism that may inhibit nuclear activity in cluster cores is the temperature of the ICM. As the ICM may be of the order of tens of megaKelvin (Fabian 1994), accretion on to galaxies is unlikely (Davies et al. 2017). In combination, these mechanisms result in galaxies in the cluster core that have an intrinsically low reservoir of cold gas (Giovannelli & Haynes 1985) and thus cannot easily fuel an AGN.

Whilst these effects are well established in clusters, they may not extend to groups. Unlike clusters, which may contain many thousands of galaxies, groups have only up to a few tens of members, and significantly lower halo masses. The dynamics of the group environment may permit more galaxy–galaxy interactions that are effective in driving gas towards the galactic nucleus within in the group centre. Furthermore, the lower halo masses of groups will result in a smaller heating effect from the virial shock acting on the intragroup medium (IGM, Grootes et al. 2017). This may allow for easier, or more rapid, accretion of the IGM on to galaxies and act as a potential fuel reservoir. Finally, the lower density of the

galaxy groups results in lower ram pressures affecting infalling galaxies (Marshall et al. 2018). Consequently RPS will be less likely to strip a galaxy of a large fraction of its gas. Ergo, these environmental differences between group and cluster galaxies may foster the presence of AGN in the cores of groups.

While galaxy groups have been shown to have a higher global AGN fraction than clusters (Shen et al. 2007; Arnold et al. 2009; Tzanavaris et al. 2014; Oh et al. 2014), it is unestablished whether the effects of position in projected phase-space seen in clusters are present or absent in groups. Where efforts have been made to study the effect of groups on AGN these studies are limited by small numbers of detected groups. This hinders the ability to stack groups to perform a phase-space analysis with any level of statistical confidence. The Galaxy And Mass Assembly survey (GAMA, Driver et al. 2011; Liske et al. 2015) is highly spectroscopically complete (98 per cent at $r < 19.8$ mag, Liske et al. 2015) making it well suited to environmental analyses of galaxies (e.g. Brough et al. 2013; Casteels et al. 2014; Robotham et al. 2014; Alpaslan et al. 2015; Davies et al. 2016; Barsanti et al. 2017; Ching et al. 2017; Gordon et al. 2017). GAMA is thus ideal for studying the lower halo mass regime of galaxy groups and has detected more than 23 000 groups with 2–316 members (Robotham et al. 2011).

In this work, we investigate the effect of the group environment on galactic nuclear activity by using spectroscopically selected AGN and version 9 of the GAMA group catalogue. We analyse prevalence of AGN as a function of group mass and position in group projected phase-space. For our analysis, we only use groups with at least five members (full details are given in Section 2.2). We are thus expanding on the work of Pimblet et al. (2013) and probing further down the group halo mass function, and, as a result of the depth of GAMA, to lower galactic stellar masses.

In Section 2, we detail the GAMA survey and the specific data used in this work. Our results are given in Section 3, and our discussion is presented in Section 4. Section 5 is a summary of our conclusions. Throughout this paper a standard flat Lambda cold dark matter cosmology is assumed with $h = 0.75$, $H_0 = 100 h \text{ km s}^{-1} \text{ Mpc}^{-1}$, $\Omega_M = 0.25$, and $\Omega_\Lambda = 0.75$.

2 DATA

2.1 Galaxy And Mass Assembly

The GAMA survey spectroscopic campaign was undertaken with the Anglo-Australian Telescope (AAT) at Siding Spring Observatory between 2008 and 2014 (Driver et al. 2011; Liske et al. 2015). During this period, spectra with a resolution of $R \approx 1300$ covering the wavelength range 3750–8850 Å were obtained using the 2dF/AAOmega spectrograph for over 250 000 galaxies (Hopkins et al. 2013). The GAMA survey footprint covers five regions of the sky totalling 286 deg² with extremely high spectroscopic completeness. Specifically, at $r < 19.8$ mag, completeness is >98 per cent in the three equatorial regions (G09, G12, G15), which we use in this work.

2.2 Galaxy groups

2.2.1 GAMA Group Catalogue, G³Cv09

The depth and completeness of GAMA naturally lends itself to the reliable detection of galaxy groups of lower mass than would be possible with a shallower and less spectroscopically complete survey. The resultant GAMA group catalogue is constructed through the use of a friends-of-friends (FoF) algorithm (Robotham et al.

2011). We use the latest version of the group catalogue, G³Cv09, which covers the three GAMA equatorial regions, and contains 75 029 galaxies in 23 654 groups with $z < 0.6$. The number of group members, N_{FoF} , ranges from 2 (14 876 groups) to 316 (Abell 1882; Owers et al. 2013).

We select the groups for use in this work to be within a suitable redshift so that we can be confident in our mass completeness, and having enough group members such that low group multiplicity does not bias our projected phase-space analysis. To determine a redshift limit to use, we use the distribution of maximum observable redshift of the GAMA galaxies at $r < 19.8$ mag, as calculated by Taylor et al. (2011). By limiting our analysis to $z < 0.15$, we are able to probe down to a stellar mass of $10^{9.9} M_{\odot}$ with 90 per cent completeness.

2.2.2 Group membership

The FoF algorithm used to determine the group membership in G³Cv09 is more reliable at detecting low-mass groups than halo-galaxy grouping methods (Robotham et al. 2011). However, this method preferentially detects group members at low projected radii (Barsanti et al. 2017), and hence will bias the results of any projected phase-space analysis conducted. To counter this, we define our own group sample membership, using the GAMA group catalogue as a starting point. Using the observed group velocity dispersion, σ_{group} , we calculate R_{200} as per (Carlberg, Yee & Ellingson 1997),

$$R_{200} = \frac{\sqrt{3}\sigma_{\text{group}}}{10H(z)}, \quad (1)$$

and the halo masses, M_{200} , using

$$M_{200} = \frac{\sigma_{\text{group}}^3}{1090^3 h(z)} 10^{15} M_{\odot} \quad (2)$$

derived by Munari et al. (2013). Using the central galaxy from the respective FoF group as our group centre, we then count galaxies within $3.5\sigma_{\text{group}}$ and $3.5R_{200}$, comparable to the analysis conducted by Pimbblet et al. (2013), as group members. When compared to mock catalogues, derived group parameters are shown to be more reliable for GAMA groups with $N_{\text{FoF}} \geq 5$ (Robotham et al. 2011), suggesting that these groups are more representative of the expected group population. We thus use only these groups as the seeds for our group sample.

At high projected separation and velocities, interloping field galaxies that are serendipitously selected in the group may be a source of substantial sample contamination (Rines et al. 2005; Oman & Hudson 2016; Owers et al. 2017). To counter this, we further require that galaxies satisfy the infall criteria of spherical Navarro–Frenk–White (NFW, Navarro, Frenk & White 1996) profiles as per the method used by Barsanti et al. (2017). That is,

$$V_{\text{infall}}(R/R_{200}) < V_{200} \sqrt{\frac{2}{R/R_{200}} \frac{\ln(1 + \kappa R/R_{200}) - (\kappa R/R_{200})/(1 + \kappa R/R_{200})}{\ln(1 + \kappa) - \kappa/(1 + \kappa)}}, \quad (3)$$

where κ is the Dolag et al. (2004) halo concentration index given by

$$\kappa(M_{200}, z) = \frac{9.59}{1 + z_{\text{group}}} \left(\frac{M_{200}}{10^{14} M_{\odot} h^{-1}} \right)^{-0.102} \quad (4)$$

z_{group} is the median redshift of the group, and $V_{200} = \sqrt{GM_{200}/R_{200}}$.

One potential complication of this method is the potential for galaxies being assigned to multiple groups. In this event, a galaxy is assigned to the group that provides the smallest value for the parameter C (Smith et al. 2004). C is given by

$$C = \frac{(cz_{\text{gal}} - cz_{\text{group}})^2}{\sigma_{\text{group}}^2} - 4 \log_{10} \left(1 - \frac{R}{R_{\text{group}}} \right), \quad (5)$$

where R is the projected separation of the galaxy from the group centre, and R_{group} is $3.5R_{200}$. We further require that at least five members are assigned to each group via this method to be counted in our projected phase-space analysis, resulting in a sample of 723 groups at $z_{\text{group}} < 0.15$.

2.2.3 Group substructure

For high-multiplicity groups, we do not wish to bias our results due to any significant substructure that may be present in the group core. To ensure this is not the case, we subject large groups to a Δ , or DS (Dressler & Shectman 1988) test for subclustering. Note that it is the centres of groups in which we are concerned about substructure. To find substructure here would indicate that the group is not a virialized structure and hence unsuitable for our analysis of projected phase-space as this may affect the likelihood of AGN to be found in this region. Moreover, such central substructure may influence the measured dynamical mass of a group. The DS test is sensitive to substructure in group sizes as low as 30 members. We therefore perform this test on groups with at least 30 members within R_{200} of the group centre. Of our 723 groups, 41 satisfy this criterion.

To apply the DS test, for each galaxy, i , the n nearest neighbours are used to determine a local mean velocity and velocity dispersion. These are then compared to the group global values and a statistic, δ , can be calculated by

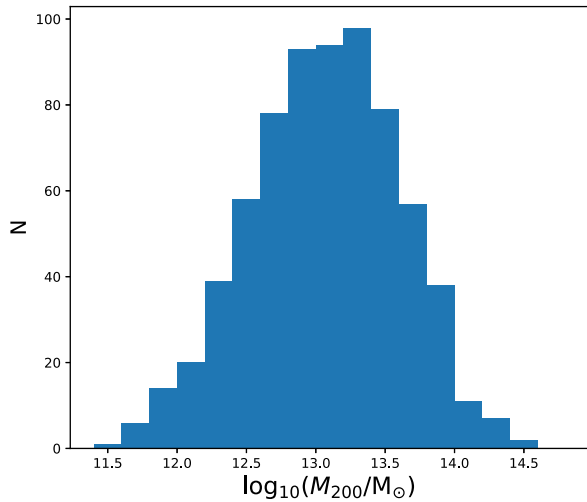
$$\delta_i^2 = \frac{n+1}{\sigma_{\text{global}}} [(v_{\text{local}} - v_{\text{global}})^2 + (\sigma_{\text{local}} - \sigma_{\text{global}})^2], \quad (6)$$

where v is the mean velocity and σ the velocity dispersion. For each group, a cumulative statistic, Δ is obtained by $\Delta = \sum \delta_i$. Pinkney et al. (1996) and Einasto et al. (2012) recommend that the number of nearest neighbours, n , be the square root of the number of galaxies used to determine the cumulative statistic, Δ , i.e. $n = \sqrt{N_{R < R_{200}}}$. A p -value for the absence of substructure is obtained by calibrating Δ by the use of Monte Carlo simulations whereby $p = N(\Delta_{\text{MC}} > \Delta_{\text{obs}})/N(\text{MC})$. Such simulations are performed by randomly shuffling the galaxy velocities, therefore removing any locally coherent velocity substructure information that is the result of dynamical substructure within the group. For our DS tests, we run 1000 Monte Carlo simulations. Given this, and the sensitivity of the DS test to substructure of the order of 1/7 of the total cluster mass (Pinkney et al. 1996), a low p -value is indicative of significant substructure. Of the 41 groups we subjected to the DS test, 18 resulted in $p < 0.01$, and were hence eliminated from the analysis.

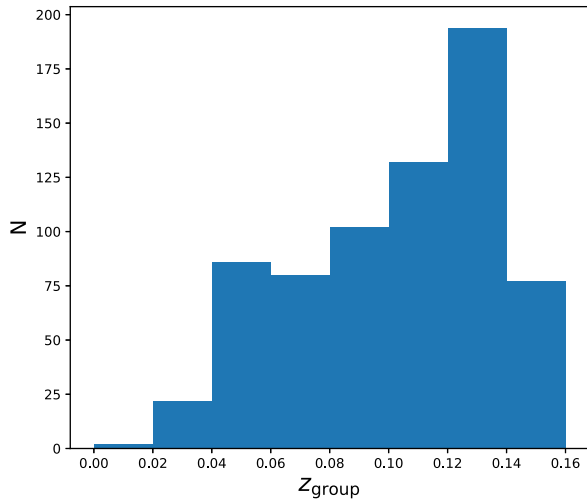
This leaves us with 7498 galaxies with $M_* > 10^{9.9} M_{\odot}$ in 695 groups of between 5 and 418 members, the distributions of the group multiplicity, velocity dispersions, and halo masses of this sample are described in Table 1, and the halo mass and redshift distributions are shown in full in Fig. 1.

Table 1. The number of group members (N), group velocity dispersion (σ_{group}), radius (R_{200}), and mass (M_{200}) of the groups used for the projected phase-space analysis in this paper. For each property, the mean, standard deviation and the 0th, 25th, 50th, 75th, and 100th percentiles are given.

Group property	μ	σ	Min	Q_1	Q_2	Q_3	Max
N	21.49	26.89	5.00	9.00	15.00	25.00	418.00
$\sigma_{\text{group}} [\text{km s}^{-1}]$	248	103	69	173	228	304	718
$R_{200} [\text{kpc } h^{-1}]$	548	226	159	381	504	675	1567
$\log_{10}(M_{200}/M_{\odot})$	13.06	0.54	11.53	12.71	13.07	13.45	14.56



(a)



(b)

Figure 1. The distributions of the halo mass (M_{200} , a) and median redshift (b) of our group sample.

2.3 AGN selection

2.3.1 A complete AGN sample

The GAMA AGN sample of Gordon et al. (2017) contains 954 broad- and narrow-line AGN, relying on the Kewley et al. (2001) criteria,

$$\log_{10} \left(\frac{[\text{O III}] \lambda 5007}{\text{H}\beta} \right) > \frac{0.61}{\log_{10} \left(\frac{[\text{N II}] \lambda 6583}{\text{H}\alpha} \right) - 0.47} + 1.19 \quad (7)$$

to classify narrow-line AGN on a Baldwin–Phillips–Terlevich (BPT, Baldwin, Phillips & Terlevich 1981) diagnostic diagram. This requires the detection of four emission lines, $\text{H}\beta$, $[\text{O III}] \lambda 5007$, $\text{H}\alpha$, $[\text{N II}] \lambda 6583$ at $S/N > 3$, and, consequently, is a conservative selection in that it prioritises sample fidelity ahead of completeness. Cid Fernandes et al. (2010) found that only forty percent of emission line galaxies (ELGs) in the ‘right wing’ and AGN areas of the BPT diagram may be detected with $S/N > 3$ in both $\text{H}\beta$ and $[\text{O III}] \lambda 5007$, and thus be selected as AGN. That is to say, in order to preserve sample fidelity, the criteria of Kewley et al. (2001) may miss a majority of narrow-line AGN.

To account for this, Cid Fernandes et al. (2010) proposed selecting narrow-line AGN on the basis of the two stronger emission lines, $\text{H}\alpha$ and $[\text{N II}] \lambda 6583$. Using these two emission lines, AGN may be selected by comparing the ratio of $[\text{N II}] \lambda 6583$ to $\text{H}\alpha$, to the equivalent width of $\text{H}\alpha$. The resultant so-called ‘WHAN’ diagram (Cid Fernandes et al. 2011) categorizes ELGs as having $\text{EW}_{\text{H}\alpha} > 3 \text{ \AA}$, and

- (i) star-forming, $\log_{10} \left(\frac{[\text{N II}] \lambda 6583}{\text{H}\alpha} \right) < -0.4$,
- (ii) weak AGN, $\log_{10} \left(\frac{[\text{N II}] \lambda 6583}{\text{H}\alpha} \right) > -0.4$ and $\text{EW}_{\text{H}\alpha} < 6 \text{ \AA}$, and
- (iii) strong AGN, $\log_{10} \left(\frac{[\text{N II}] \lambda 6583}{\text{H}\alpha} \right) > -0.4$ and $\text{EW}_{\text{H}\alpha} > 6 \text{ \AA}$,

where the category ‘weak AGNs’, are the less powerful counterparts to the ‘strong AGN’, but where the AGN is still considered to be the dominant ionization mechanism (Cid Fernandes et al. 2011). Galaxies with $\text{EW}_{\text{H}\alpha} < 3 \text{ \AA}$ are considered to be passive in nature.

To select our AGN using the WHAN criteria, we select the best spectrum available for galaxies in our group sample with $nQ \geq 3$, i.e. greater than 90 per cent confidence in the measured redshift (Driver et al. 2011; Liske et al. 2015). We use only spectra with $\text{H}\alpha$ and $[\text{N II}] \lambda 6583$ in emission. This requires that the Gaussian has been successfully fit to each line in SPEC LINE SFR v05, the values and errors on flux and equivalent widths to be greater than zero, and the signal to noise ratio (S/N) on both lines is greater than three. For AAT obtained spectra, we use only those spectra unaffected by fringing.¹ Furthermore, it is difficult to obtain reliable mass estimates for broad-line AGN (Gordon et al. 2017) and we hence exclude them from this analysis. Thus, we only use galaxies that do not have a broad component to the $\text{H}\alpha$ line, i.e. a single Gaussian fit is preferred.

These criteria select 2864 ELGs from the 7498 in our group sample. In order to account for Balmer absorption, the flux and equivalent width of the $\text{H}\alpha$ line are corrected, as per Hopkins et al. (2013), by

$$S_{\text{H}\alpha, \text{intrinsic}} = S_{\text{H}\alpha, \text{observed}} \left(\frac{\text{EW}_{\text{H}\alpha} + 2.5 \text{ \AA}}{\text{EW}_{\text{H}\alpha}} \right). \quad (8)$$

The WHAN diagram of the ELGs is shown in Fig. 2. Note, that because of the strict criteria imposed to ensure the reliability of the detected emission lines, the passive galaxy section of this diagram is barren.

2.3.2 Sample contamination

Although such an AGN selection will be more complete than more conservative methods, the level of contamination from galaxies

¹ Approximately 5 per cent of AAOmega spectra suffer from a time-dependent fringing artefact (Hopkins et al. 2013); this is flagged in the GAMA catalogue AATSPECALLV27.

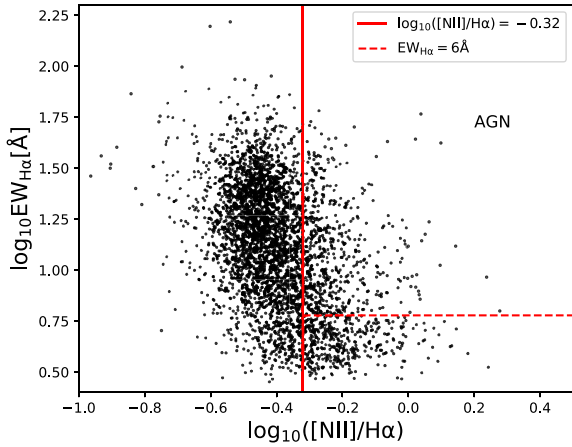


Figure 2. A WHAN diagram of the ELGs selected in our group sample. The horizontal red dashed line is used to segregate AGN from weak AGN composites, and LIERs. The vertical red line is $\log_{10}([\text{N II}]\lambda 6583/\text{H}\alpha) = -0.32$, which defines the boundary between the star-forming and AGN regions of the plot. To be classified as an AGN a galaxy must be located above the red dashed line and to the right-hand side of the red solid line. Note the absence of galaxies with $\log_{10}(\text{EW}_{\text{H}\alpha}/\text{\AA}) < 0.5$, a consequence of the stringent selection criteria applied.

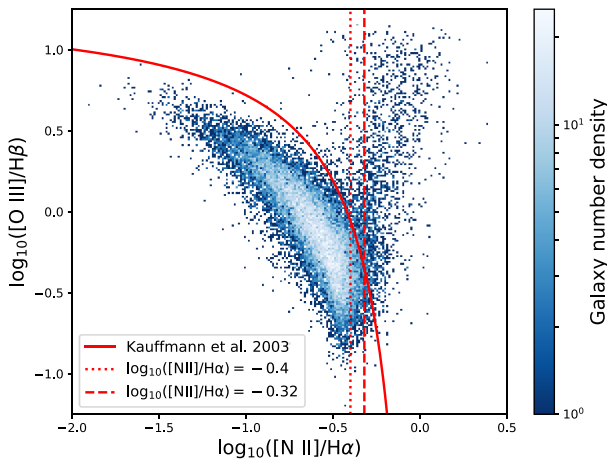


Figure 3. A BPT diagram of the ELGs in GAMA. The Kauffmann et al. (2003) line is plotted as the solid red curve. The red dotted line shows $\log_{10}([\text{N II}]\lambda 6583/\text{H}\alpha) = -0.4$, often used to select AGN in WHAN diagnostic criteria. The red dashed line shows $\log_{10}([\text{N II}]\lambda 6583/\text{H}\alpha) = -0.32$ used to select AGN in this work. The large fraction of star-forming galaxies located between the two vertical lines is readily apparent.

ionized by a non-AGN source will naturally be higher. Given that the WHAN and BPT diagrams share an axis, this contamination can be visualized by over-plotting the Cid Fernandes et al. (2010) AGN/SF segregation on to the BPT (See Fig. 3). To quantify, and minimize this, one can compare the classifications on both the WHAN and BPT of galaxies where all four BPT lines are detected with $S/N > 3$. For this, we classify those galaxies satisfying the Kewley et al. (2001) criteria (equation 7) as AGN, those satisfying the Kauffmann et al. (2003) criteria,

$$\log_{10}\left(\frac{[\text{O III}]\lambda 5007}{\text{H}\beta}\right) < \frac{0.61}{\log_{10}\left(\frac{[\text{N II}]\lambda 6583}{\text{H}\alpha}\right) - 0.05} + 1.3 \quad (9)$$

as star-forming galaxies, and those galaxies not satisfying either criteria as composite sources.

Applying these criteria to WHAN selected AGN, shows that contamination of the AGN population by star formers is limited to those AGN with the lowest $[\text{N II}]\lambda 6583/\text{H}\alpha$ ratios. The $[\text{N II}]\lambda 6583/\text{H}\alpha$ used in the WHAN diagram is derived from the Stasińska et al. (2006) AGN/star-forming segregation. Transposing the more conservative Kauffmann et al. (2003) AGN/star-forming segregation on to the WHAN diagram would result in galaxies with $\log_{10}([\text{N II}]\lambda 6583/\text{H}\alpha) < -0.32$ being classified as star forming. Indeed, when only galaxies with $-0.4 < \log_{10}([\text{N II}]\lambda 6583/\text{H}\alpha) < -0.32$ are considered, star formers make up $75.88^{+1.06}_{-1.13}$ per cent of the population with all four BPT lines at $S/N > 3$. When only galaxies with $\log_{10}([\text{N II}]\lambda 6583/\text{H}\alpha) > -0.32$ are considered, the contamination of the sample by star-forming galaxies is reduced to $11.07^{+0.99}_{-0.85}$ per cent. Given the decreasing detections of all four BPT lines with increasing $[\text{N II}]\lambda 6583/\text{H}\alpha$ ratio shown in Cid Fernandes et al. (2010), we take this as an upper limit on the star-forming contamination of the ELG sample.

While altering the minimum $[\text{N II}]\lambda 6583/\text{H}\alpha$ ratio of our sample will reduce the contamination from pure star-forming sources, the contribution from the composite population is substantial. There are various arguments as to the nature of this population with a variety of sources thought to contribute. Kewley et al. (2001) argue that galaxies can be classified as a composite solely as the result of ionization from an extreme starburst phase. However, the sample contamination from such sources will be minimal. Taking the Poggianti & Wu (2000) e(b) classification as a proxy for the starburst population, we find these galaxies constitute < 1 per cent of the ELG population in GAMA. Ionization from post-AGB stars is likely to be a considerable source of contamination for the composite population. Furthermore, the Kewley et al. (2001) AGN population will be contaminated by low-ionization emission regions (LIERs). Both of these contaminants present with weak hydrogen lines (fig. 2 of Sanchez et al. 2017; Marshall et al. 2018), and thus their contribution to an AGN selection can be minimized by selecting AGN only with strong $\text{H}\alpha$, i.e. $\text{EW} > 6 \text{\AA}$, emission.

To achieve a balance between high sample completeness and fidelity, we select our AGN using a conservative variant of the WHAN diagnostic criteria. Specifically, we classify as AGN galaxies with $\log_{10}([\text{N II}]\lambda 6583/\text{H}\alpha) > -0.32$ and $\text{EW}_{\text{H}\alpha} > 6 \text{\AA}$. This produces a sample of 451 AGN in our selected groups.

3 OBSERVATIONS AND ANALYSIS

3.1 The group AGN fraction

Taking the group population as a whole, we find that AGN constitute $6.01^{+0.29}_{-0.26}$ per cent of the galaxies more massive than $10^{9.9} M_{\odot}$ in our sample. Given that the masses of our groups span three orders of magnitude (See Table 1), we wish to determine whether this AGN fraction is dependent on the mass of the group. In Fig. 4, we split our group sample in to four bins of M_{200} . We show that the AGN fraction is approximately flat at a halo mass of $\log_{10}(M_{200}/M_{\odot}) > 13$. Lower mass groups have a higher, if not significantly so, AGN fraction than higher mass groups. For all fractional calculations, both here and throughout this paper, the errors are binomial as per Cameron (2011).

3.2 AGN in group projected phase-space

It has been shown that for massive clusters, AGNs are preferentially found in the infall regions of those clusters, and are less likely to be found in the cluster centre (Haines et al. 2012; Pimblet et al.

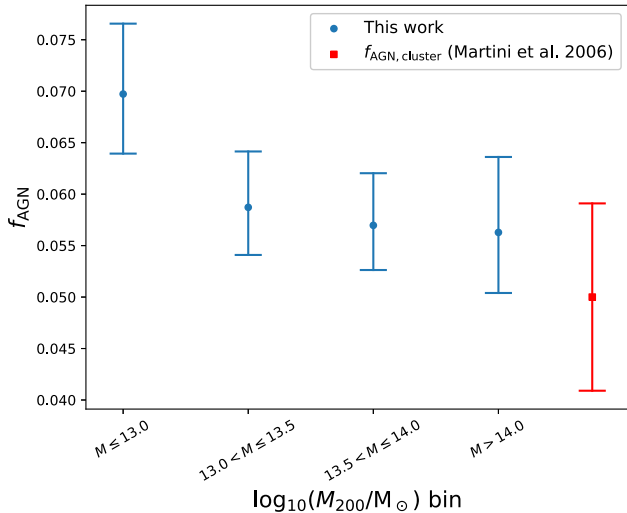


Figure 4. The fraction of the galaxy population hosting an AGN in bins of group mass, M_{200} . The AGN fraction is flat for $M_{200} > 10^{13.0} M_{\odot}$, and marginally elevated at lower halo masses. The red square shows the AGN fraction in clusters, and 1σ errors, obtained from Martini et al. (2006) for comparison.

2013). To test if this is the case in lower mass groups, we stack our selected groups into one large ‘supergroup’ of 7498 galaxies. We then analyse the positions of those galaxies in the projected radius versus velocity difference phase-space plane. In order for this projected phase-space to be useable for our stacked group, we must normalize the dimensions. For the projected separation, we use the projected separation of a galaxy from the iterative centre of the group, and normalize by R_{200} . To calculate the velocity difference, we use the difference between the redshift of the galaxy and the median redshift of the group, i.e. $\Delta v = c(z_{\text{gal}} - z_{\text{group}})/(1 + z_{\text{group}})$. This is normalized by the group velocity dispersion.

Ehler et al. (2013) and Pimblet et al. (2013) showed that AGN fraction increases with projected radius from the cluster centre. Given this established result for clusters, we test whether the same result holds for galaxy groups. In Fig. 5, we show the same trend for our group sample. In order to test whether this effect is biased by the large mass range of groups in our sample, we repeat this test for the upper and lower quartiles of the mass distribution of our group sample. This shows that the low AGN fraction inside R_{200} is driven by high-mass groups, where the AGN fraction is lower at $R < R_{200}$ at 2.9σ confidence.

In Fig. 6, we show the relative number densities of galaxies and AGN in projected phase-space and the expected infall curve from the work of Oman, Hudson & Behroozi (2013). This curve is defined as

$$\frac{|v|}{\sigma_{\text{group,3D}}} = -\frac{4}{3} \frac{R}{R_{\text{virial}}} + 2, \quad (10)$$

where $R_{\text{virial}} = \frac{2.5}{2.2} R_{200}$ (Oman et al. 2013), and $\sigma_{\text{group,3D}}$ is the three-dimensional equivalent of σ_{group} , i.e. $\sqrt{3}\sigma_{\text{group}}$ (Barsanti et al. 2017). By comparing with this expected infall curve, Fig. 6 shows qualitatively that, as one might expect for virialized structures, the number density of galaxies is higher below this curve. The number density of AGN, however, is seen to be more widely distributed, and the AGN fraction is highest in the infall regions, i.e. above the Oman et al. (2013) curve.

The AGN fractions calculated for the bins in Fig. 6 have a median absolute error of 0.02. To reduce this error and better quantify

the difference in AGN triggering likelihood with environment, we calculate the AGN fractions for the virialized and infalling galaxy populations as defined by equation (10). For our stacked group, the AGN fraction in the virialized region is $4.50^{+0.36}_{-0.32}$ per cent compared to $7.56^{+0.46}_{-0.41}$ per cent in the infall regions. Across our sample, AGNs are more likely to be found in infalling galaxies with 3.9σ confidence.

As with the overall group AGN fraction, and the effect of projected separation from the group centre, we wish to test whether this preference for AGN to be found in the infalling population is driven by groups in a particular mass regime. In Fig. 7, we show the galaxies and AGN in projected phase-space for the lower and upper quartiles, in terms of halo mass, of our sample. We also show the histograms for active and inactive galaxies in each of the projected phase-space dimensions, which clearly show a difference in the distribution of AGN at these halo mass regimes. To quantify this, we attempt to constrain at what group mass the environmental transition occurs. In Fig. 8, we bin the mass range of our sample and compare the likelihood of virialized and infalling galaxies hosting an AGN. This shows a decreasing AGN fraction amongst virialized galaxies with increasing group mass. At $\log_{10}(M_{200}/M_{\odot}) > 13.50$, the observed AGN deficit in the group centre becomes significant at the 3.6σ level. For group halo masses greater than $10^{13.5} M_{\odot}$, $3.70^{+0.50}_{-0.40}$ per cent of the virialized galaxy population host an AGN, in contrast to $7.55^{+0.66}_{-0.57}$ per cent of the infalling population.

4 DISCUSSION

4.1 AGN in large-scale structure

The dynamics of large-scale structure (LSS) change with structure size. For instance, one would not expect that a galaxy pair would have a similar kinematic environment to a larger group of many tens of members, the latter of which may well be virialized. Galaxy pairs, especially a close pair, and small groups of only a few members are likely to be directly interacting (Hickson 1997; Robotham et al. 2014), a widely considered trigger for nuclear activity within galaxies (e.g. Sanders et al. 1988; Krongold et al. 2002; Ellison et al. 2011). This is supported by observations that both pairs and compact groups exhibit higher nuclear activity compared to field environments, with AGN fractions approaching ~ 20 per cent in the closest pairs (Rubin et al. 1991; Menon 1995; Ellison et al. 2011).

Pairs and compact groups represent the smallest supergalactic structures in the Universe. At the other end of the scale are massive clusters. In contrast to smaller structures, clusters have AGN fractions of just ~ 5 per cent (Martini et al. 2006; Arnold et al. 2009). This is lower than the field AGN fraction of 8 ± 0.13 per cent² (Woods & Geller 2007). This could suggest that the environmental changes associated with moving up the LSS mass function first act to increase AGN triggering opportunities through direct interaction, before inhibiting AGN triggering in high mass structures.

As a mid-point in the LSS mass function, galaxy groups should therefore sit between small structures such as pairs and compact groups, and clusters in terms of AGN fraction. Indeed prior observations have shown galaxy groups to have AGN fractions in the range ~ 7 – 9 per cent (Shen et al. 2007; Arnold et al. 2009; Oh et al. 2014; Tzanavaris et al. 2014). Our own observations are broadly consistent with this picture. We observe an AGN fraction

² We have extrapolated the uncertainty on this value from table 1 of Woods & Geller (2007).

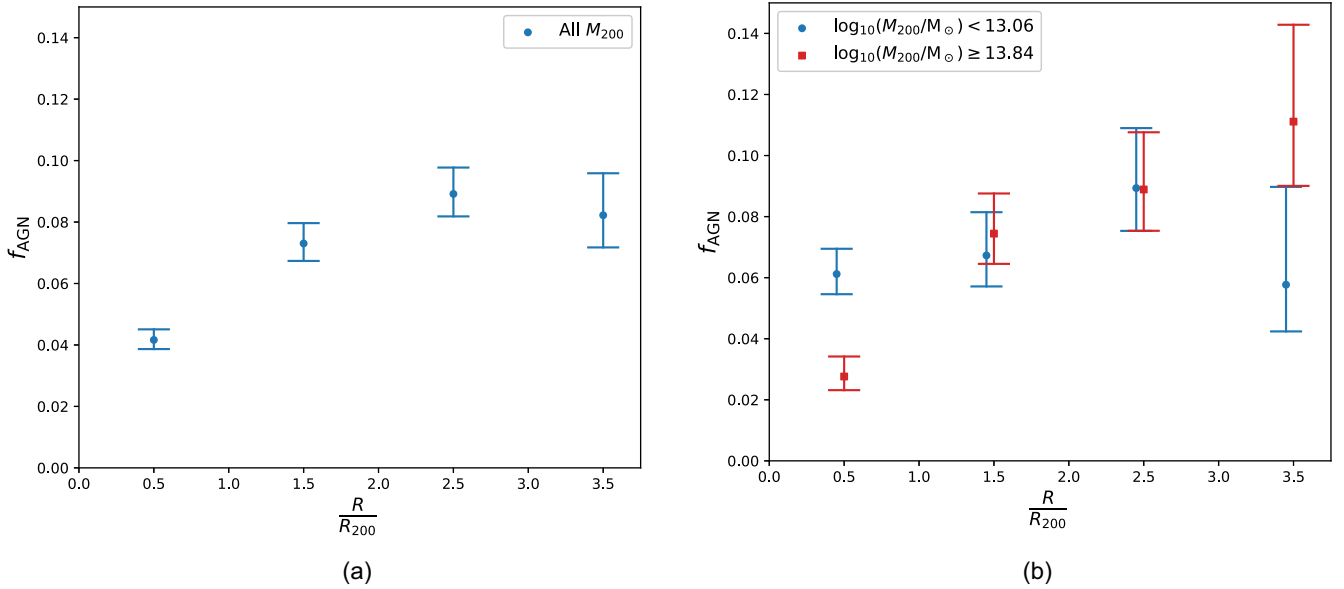


Figure 5. The effect of projected separation from group centre on AGN fraction. In panel (a) the entire group sample is considered. Panel (b) splits the sample into the upper and lower quartiles of the group mass distribution, showing that low-mass groups do not have the deficit of centrally located AGN seen in high-mass groups and clusters (Ehler et al. 2013; Pimbblet et al. 2013). For panel (b) blue circles represent groups with $\log_{10}(M_{200}/M_{\odot}) < 13.06$, while groups with $\log_{10}(M_{200}/M_{\odot}) > 13.84$ are shown by red squares, these are marginally offset along the x-axis for clarity. For both panels, the bin width is R_{200} for all bins.

of $6.01^{+0.29}_{-0.26}$ per cent, although we note that this covers the mass range of our group sample, i.e. $11.53 \leq \log_{10}(M_{200}/M_{\odot}) \leq 14.56$. Consequently, this may be driven by the high mass end of our group sample. Taking only the lowest quartile of the group mass range, the AGN fraction is $6.68^{+0.62}_{-0.53}$ per cent. This is perfectly consistent with the overall value observed in our sample, but is closer to the expected value from previous studies.

4.2 Galaxy location within the group structure

As well as the galactic environment changing with group mass, the environmental conditions are a function of location within the group. Extending on the work of Haines et al. (2012) and Pimbblet et al. (2013), we have shown in Fig. 5 that, although the radial AGN fraction of our groups decreases inside R_{200} , this effect is driven by high-mass groups. For low-mass groups, we show the AGN fraction out to $3.5R_{200}$ to be approximately flat. This suggests that the central regions of low-mass groups are similar to the more extended regions of those groups in terms of their ability to host AGN.

To conduct a more physically motivated analysis, we use the criteria of Oman et al. (2013) to split the groups into infalling and virialized populations. This shows that AGNs are significantly ($\sim 3.9\sigma$) more likely to be found in infalling galaxies than virialized galaxies. As with the radial AGN fraction, this is primarily driven by the high-mass groups in our sample. Fig. 8 shows the infall AGN fraction remains flat at ~ 7.5 per cent across the mass range of our group sample, comparable to the field AGN fraction (Woods & Geller 2007). This is suggestive that the act of falling into a group does not increase the likelihood of a galaxy hosting an AGN. The AGN fraction in the virialized region of the groups however, is shown to decrease with increasing halo mass. This effect becomes significant at the 3.6σ level for groups with $M_{200} > 10^{13.5} M_{\odot}$, where only ~ 3.5 per cent of virialized galaxies host an AGN. That is to say, as one might expect, our high-mass groups start to show

the same observational properties with regard to AGN fostering that has been previously observed in clusters (Gilmour et al. 2007; Gavazzi et al. 2011; Haines et al. 2012; Pimbblet & Jensen 2012; Pimbblet et al. 2013).

The decreasing AGN fraction in virialized galaxies with increasing group mass leads to the inference that the physics of the group core evolves with group mass. Indeed, this should be expected if groups are simply low-mass and less evolved analogues of clusters. In relaxed clusters, the cores are virialized and consequently the frequency of low-speed interactions that may act as a trigger for AGN is reduced. As a group evolves into a cluster one would expect the dominance of this effect to increase, and consequently this mechanism may well play a role in the low virialized AGN fraction we see in our high-mass groups.

A second mechanism that may contribute to the absence of AGN in the centres of large groups is the temperature of the IGM. In clusters, it has been suggested that the high temperature of the ICM prevents the matter from being accreted on to a galaxy and hence starves any potential AGN of a fuel supply (Davis & Bureau 2016; Davies et al. 2017). As one goes up the group mass function, the IGM temperature increases (Shimizu et al. 2003), and hence so does the effectiveness of this mechanism. Given that we see no substantial lack of AGN in the centres of low-mass groups, our observations may support such a model.

The inhibition of nuclear activity in the virialized region of phase-space of large groups may also be caused by RPS. The infall regions of clusters have been shown (Marshall et al. 2018) to provide the appropriate gas pressures to compress and destabilise intragalactic gas (Schulz & Struck 2001; Tonnesen & Bryan 2009), potentially fuelling nuclear activity (Marshall et al. 2018). In the cores of clusters however, galaxies are subject to higher ram pressures that not only disrupt the internal galactic gas, but strip it from the galaxy (e.g. Kenney et al. 2004). Given that one would not expect the intense ram pressures required to strip a galaxy of gas in small

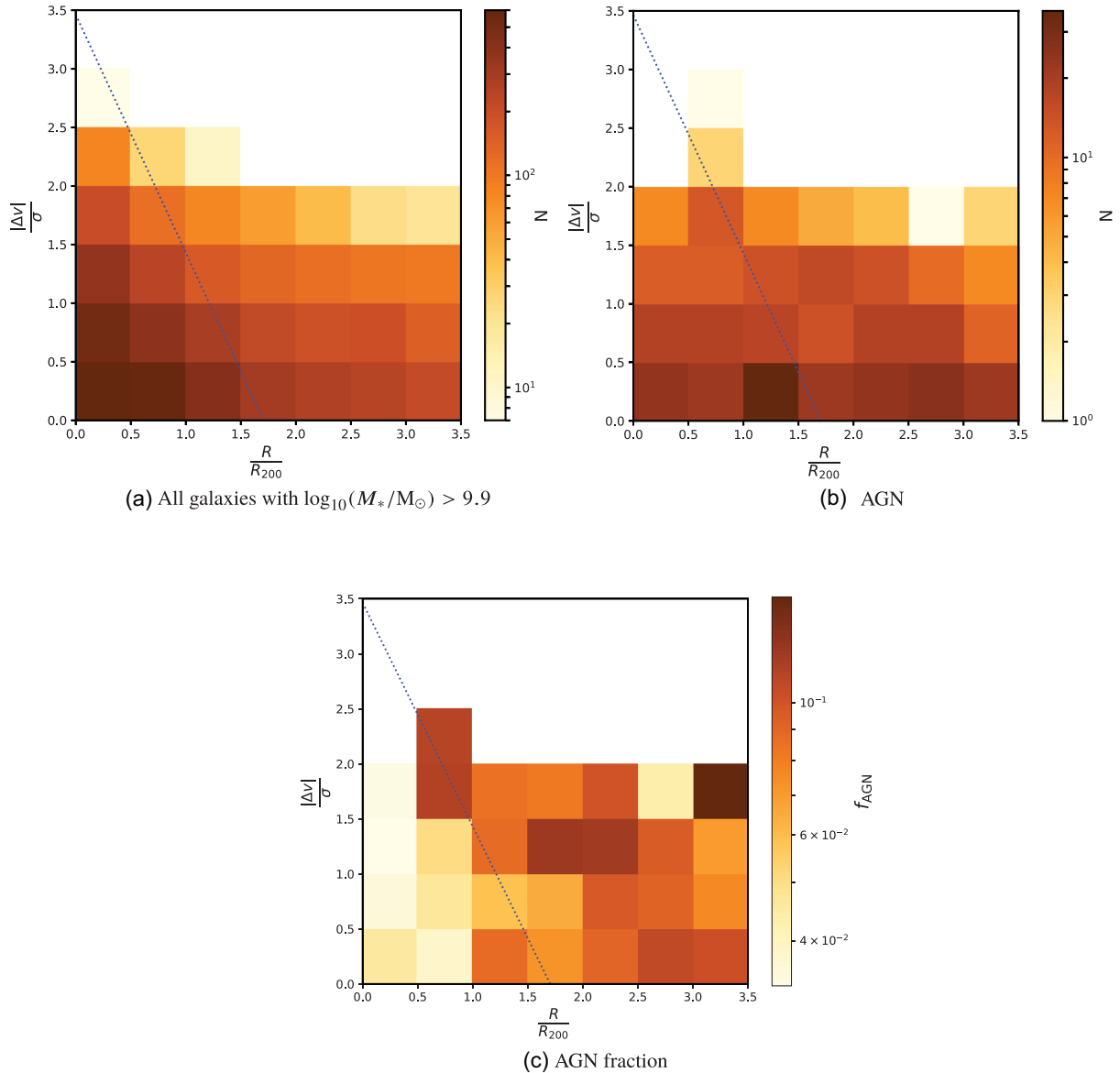


Figure 6. Two dimensional histograms showing the projected phase-space distributions of our stacked group of 7498 galaxies. Panel (a) shows the number density of all galaxies, panel (b) shows the number density of AGN, and panel (c) shows the AGN fraction. The blue dotted line shows the modelled infall curve of Oman et al. (2013). The median absolute error for the AGN fractions in panel (c) is 0.02.

groups, our observation of no AGN deficit in the central region of projected phase-space for low-mass groups is consistent with extreme RPS being a plausible mechanism for preventing nuclear activity in cluster cores.

The phase-space projections of galaxies within groups and clusters explain why the AGN fraction of the structure as a whole is lower than the AGN fraction in the field. If one considers only the infall region of the structure, the AGN fraction is shown to be a flat function of group halo mass (see red squares in Fig. 8). Combining the AGN fraction in the infall region for all our groups to reduce the uncertainty gives an AGN fraction of ~ 7.5 per cent, and is consistent with the AGN fraction in the field (Woods & Geller 2007). However, if one then takes into account the core region of the cluster with its AGN deficit, this will act to reduce the overall AGN fraction. In low-mass groups where this effect is not observed, the infall AGN fraction is similar to the core AGN fraction, and thus similar to the field value.

4.3 A comparison to radio AGN, star-forming galaxies, and the passive population

The AGN used in this analysis have been selected optically, and hence their SMBH is accreting matter in a radiatively efficient manner. Such an accretion mode requires a cold gas fuel reservoir. In contrast, the SMBHs of radio selected AGN may inefficiently accrete matter whilst still powering the AGN. This inefficient accretion does not require a supply of cold gas, and the black hole may be ‘drip-fed’ by either internal or external mechanisms (Hardcastle et al. 2007; Best & Heckman 2012; Ellison, Patton & Hickox 2015). Consequently, the environmental effects inhibiting optical AGN in the cores of massive structures may not inhibit radio AGN. Indeed, the majority of low-powered radio AGNs are found in the central galaxies in groups and clusters (Best et al. 2007; Ching et al. 2017). Therefore, these observations can only be used to draw conclusions about the efficiently accreting AGN population.

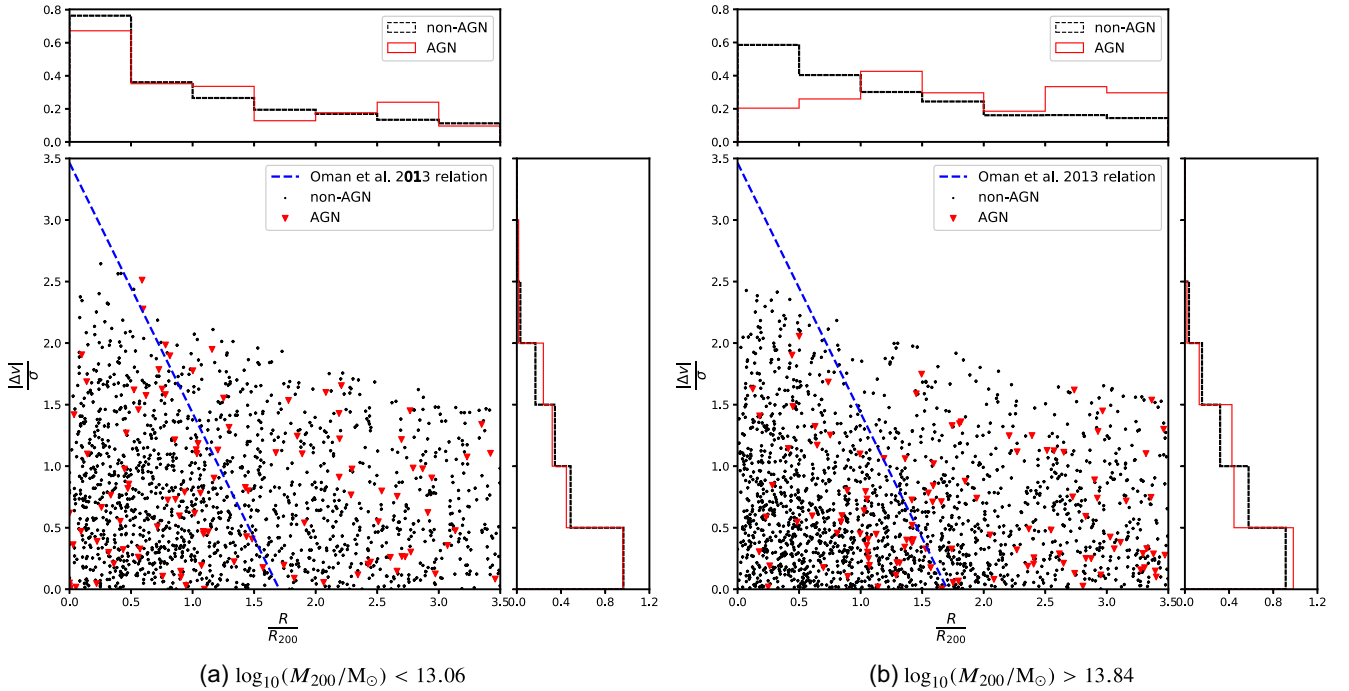


Figure 7. The projected phase-space diagrams and histograms for groups in the lower (panel a) and upper (panel b) quartiles of the group halo mass distribution. Inactive galaxies are represented by black dots in the phase-space diagram and black dashed line in the histograms, and AGNs are represented by red triangles and red solid lines in these plots, respectively. The blue dashed line marks the Oman et al. (2013) infall curve. Panel (b) clearly shows a low number of AGN at low projected radii relative to the inactive population.

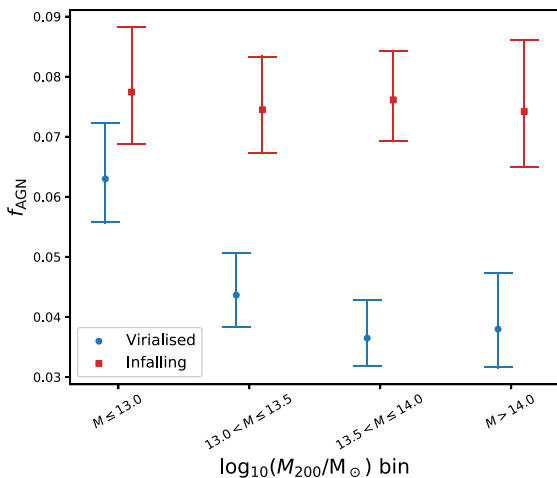


Figure 8. A comparison of the AGN fractions of the virialized and infalling galaxy populations defined by equation (10) (Oman et al. 2013). Blue circles show the virialized AGN fraction, which decreases with halo mass for $\log_{10}(M_{200}/M_{\odot}) < 13.5$. The infalling AGN fraction is represented by red squares and is flat across all halo masses in our sample. As with Fig. 5 a marginal x -axis offset is used for the two populations to improve clarity.

Star-forming galaxies, like optically selected AGN, require a fuel supply of cold gas. At the centres of massive groups, should that gas have been stripped on infall, and the IGM be too hot to accrete cold gas, then this will lead to the strangulation of star formation as well as reducing the AGN fraction in the group centre. Indeed, this effect is seen in massive clusters (Lopes, Ribeiro & Rembold 2017). Additionally, Barsanti et al. (2017) observe this effect with the fraction of star-forming galaxies increasing in groups with R/R_{200} . Although their halo mass bins are larger than ours, their

group sample shows a higher fraction of star-forming galaxies at small projected radii than their cluster sample (see fig. 5 of Barsanti et al. 2017). This is consistent with what might be expected based on our demonstration of the importance of halo mass for galaxy nuclear activity. Furthermore, both Lopes et al. (2017) and Barsanti et al. (2017) observe the opposite effect for passive galaxies, with the passive population being more centrally located. As would be expected based on our observations, this effect is stronger in clusters than groups.

4.4 Accounting for potential sources of bias

4.4.1 Stellar mass

The likelihood of a galaxy hosting an AGN increases with stellar mass (Pimblet & Jensen 2012; Pimblet et al. 2013; Lopes et al. 2017; Wang et al. 2017). Given that the central galaxies in groups are the most massive, the deficit of AGN in the cores of massive groups and clusters is unlikely to be a stellar mass bias. Moreover, if a dominant stellar mass bias were at play, one would expect to see the opposite observation. However, in low-mass groups AGNs are observed in the virialized region as frequently as in the infalling population. It is therefore necessary to confirm that the stellar mass distribution of galaxies within our group sample is not dependent in halo mass. In Fig. 9, we show the median stellar mass of galaxies within the same halo mass bins used in Fig. 8, demonstrating there is no difference in the stellar mass distributions of our high and low-mass groups.

4.4.2 Group selection

We have taken care throughout this work to ensure that bias from group selection effects is minimal in our results. None the less,

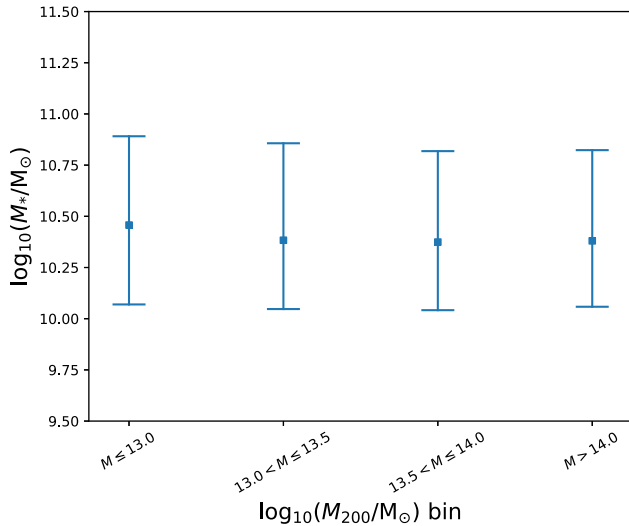


Figure 9. The median stellar mass of galaxies with $\log_{10}(M_*/M_{\odot}) > 9.9$ with group halo mass. Across the halo mass range of our sample there is no variation in the median galactic stellar mass, eliminating this as a potential source of bias for our observations. The error bars represent the 16th and 84th percentiles of the stellar mass distribution in each halo mass bin, and thus represent 68 per cent of the population.

as with any observational work, one must consider whether such effects may drive a result. FoF algorithms are reliable but may under select from the extended group structure (Barsanti et al. 2017), whereas methods such as ours that select based on a radius and velocity are prone to contamination from field galaxies. That is to say, such methods prioritise completeness over fidelity (Rines et al. 2005; Oman & Hudson 2016).

In this work, to reduce the contamination of the group sample by interloping field galaxies, we exclude from selection galaxies that fall outside the NFW infall radius predicted for a group (see Section 2.2). However, by taking this approach there is every chance of excluding high-velocity infalling galaxies that genuinely are part of the group. To test whether this affected our results, we reran the analysis on a group selection that did not account for the NFW profile. That is to say, group membership was simply defined as $R < 3.5R_{200}$; $|\Delta v| < 3.5\sigma_{\text{group}}$. This had no significant effect on our results with high-mass groups having a central AGN deficit at $\sim 4\sigma$ confidence.

To select our group members using the method described in Section 2.2.2, the centre of the group was chosen to be the galaxy that was central galaxy in corresponding FoF group (see section 4.2 of Robotham et al. 2011). The logical alternative to this would be to centre the group selection on the brightest group galaxy (BGG). In 95 per cent of cases for groups with $N_{\text{FoF}} \geq 5$, as we require for our group selection, the BGG was also the central galaxy in the group. Given this substantial overlap, we would expect altering the group selection in this way to have little effect on our results. To be certain of this, we reselected our groups using the BGG as the group centre. This resulted in a sample of 7482 galaxies with $\log_{10}(M_*/M_{\odot}) > 9.9$, of which 452 host an AGN. Redoing our analysis on this sample produced the same results as for the group selection centred on the central galaxy of the corresponding FoF group.

Of final note on the group selection, is the calculation of the halo masses, M_{200} . As described in Section 2.2, we calculate our halo masses using the scaling relation of Munari et al. (2013, see

equation 2), and thus $M_{200} \propto \sigma^3$ as would be expected from the virial theorem. Observations using weak gravitational lensing support a scaling relation with a shallower slope, $M_{200} \propto \sigma^{\sim 2}$ (Han et al. 2015; Viola et al. 2015). This weaker dependency, however, may not be accurate at the lower halo masses explored in this work. Viola et al. (2015) note that their selection criteria may result in an overestimate of the halo mass for groups with low-velocity, and thus reduce the exponent of the relation. Given this potential bias in the low-mass regime from weak-lensing derived observations, it is prudent for us to use a scaling relation consistent with the virial theorem.

4.4.3 The infalling population

Additionally, one must question whether our definition of the infalling and virialized populations may bias our results. We chose to use a physically motivated definition based on the work of Oman et al. (2013). This was based on N -body simulations and the result extrapolated into the projected phase-space plane. An independent test would be to compare our results directly with prior observations, and indeed our radial AGN fractions binned by group halo mass (see Fig. 5) support our conclusions in this regard.

Further support of our results is obtained when we compare directly to Haines et al. (2012) who found no AGN within $0.4R/R_{500}$, and $0.8|\Delta v|/\sigma$ of the cluster centre. Transposing these criteria on to our projected phase-space plane defines a region $R < 0.26R_{200}$; $|\Delta v| < 0.8\sigma_{\text{group}}$. When comparing the fraction of AGN inside this region to that outside, we find that at $M_{200} > 10^{13.5} M_{\odot}$ there is a deficit of AGN in this central region at the 2.5σ level. As with our other results, lower group masses do not show this effect.

5 CONCLUSIONS

We have exploited the depth and spectroscopic completeness, 98 per cent at $r < 19.8$ mag, of the GAMA survey (Driver et al. 2011; Liske et al. 2015) to probe the halo mass function in order to test the affect of group environment on AGN. We investigated the effect of galaxy position, both radially and within projected phase-space on AGN prevalence. Further to this, by binning our group sample by halo mass, we demonstrate the evolution of a preferential region for AGN fostering within the group projected phase-space. Our main findings are as follows.

(i) The AGN fraction within our group sample is $6.01^{+0.29}_{-0.26}$ per cent, marginally lower than previous studies have found in groups. We attribute this to the large mass range covered by our sample. Although when split by halo mass the group AGN fraction is approximately flat, for the 25 per cent of our galaxies in the lowest mass groups, $M_{200} < 10^{13.06} M_{\odot}$, the AGN fraction is $6.68^{+0.62}_{-0.53}$ per cent. This is consistent with prior observations of the group AGN fraction (Shen et al. 2007; Arnold et al. 2009; Oh et al. 2014; Tzanavaris et al. 2014).

(ii) We find the AGN fraction as a function of projected separation is flat for low-mass groups. For high-mass groups however, the AGN fraction is noticeably reduced at $R < R_{200}$, consistent with the findings of Ehlert et al. (2013); Pimblet et al. (2013) for clusters.

(iii) Using the projected phase-space to split the galaxies into virialized and infalling populations as per Oman et al. (2013, see equation 10), we show that low-mass groups do not experience the same deficit of AGN in their cores as do high-mass groups and clusters (Gilmour et al. 2007; Gavazzi et al. 2011; Haines et al. 2012).

(iv) Across the halo mass range of our group sample, the infalling AGN fraction is comparable to the field AGN fraction, indicating that there is no excess of AGN triggering on infall in to groups.

(v) We demonstrate the evolution of group cores from an environment that supports AGN at low halo masses, to one which inhibits nuclear activity at halo masses greater than $10^{13.5} M_{\odot}$ (see Fig. 8).

ACKNOWLEDGEMENTS

The authors take this opportunity to thank the anonymous referee for their constructive comments. YAG acknowledges the financial support of the University of Hull through an internally funded PhD studentship that has enabled this research to be undertaken. KAP acknowledge the support of Science and Technology Facilities Council (STFC), through the University of Hull's Consolidated Grant ST/R000840/1. MSO acknowledges the funding support from the Australian Research Council through a Future Fellowship (FT140100255).

GAMA is a joint European-Australasian project based around a spectroscopic campaign using the AAT. The GAMA input catalogue is based on data taken from the Sloan Digital Sky Survey and the UKIRT Infrared Deep Sky Survey. Complementary imaging of the GAMA regions is being obtained by a number of independent survey programmes including GALEX MIS, VST KiDS, VISTA VIKING, WISE, Herschel-ATLAS, GMRT, and ASKAP providing UV to radio coverage. GAMA is funded by the STFC (UK), the ARC (Australia), the AAO, and the participating institutions. The GAMA website is <http://www.gama-survey.org/>.

Funding for SDSS-III has been provided by the Alfred P. Sloan Foundation, the Participating Institutions, the National Science Foundation, and the U.S. Department of Energy Office of Science. The SDSS-III web site is <http://www.sdss3.org/>.

SDSS-III is managed by the Astrophysical Research Consortium for the Participating Institutions of the SDSS-III Collaboration including the University of Arizona, the Brazilian Participation Group, Brookhaven National Laboratory, Carnegie Mellon University, University of Florida, the French Participation Group, the German Participation Group, Harvard University, the Instituto de Astrofísica de Canarias, the Michigan State/Notre Dame/JINA Participation Group, Johns Hopkins University, Lawrence Berkeley National Laboratory, Max Planck Institute for Astrophysics, Max Planck Institute for Extraterrestrial Physics, New Mexico State University, New York University, Ohio State University, Pennsylvania State University, University of Portsmouth, Princeton University, the Spanish Participation Group, University of Tokyo, University of Utah, Vanderbilt University, University of Virginia, University of Washington, and Yale University.

This research made use of Astropy, a community-developed core PYTHON package for Astronomy (Astropy Collaboration 2013).

REFERENCES

Alonso M. S., Lambas D. G., Tissera P., Coldwell G., 2007, *MNRAS*, 375, 1017
 Alpaslan M. et al., 2015, *MNRAS*, 451, 3249
 Arnold T. J., Martini P., Mulchaey J. S., Berti A., Jeltema T. E., 2009, *ApJ*, 707, 1691
 Astropy Collaboration, 2013, *A&A*, 558, A33
 Baldwin J. A., Phillips M. M., Terlevich R., 1981, *PASP*, 93, 5
 Barsanti S., Owers M. S., Brough S., Davies L. J. M., Holwerda B. W., Pimbblet K. A., Loveday J., 2017, *ApJ*, in press

Best P. N., Heckman T. M., 2012, *MNRAS*, 421, 1569
 Best P. N., Von Der Linden A., Kauffmann G., Heckman T. M., Kaiser C. R., 2007, *MNRAS*, 379, 894
 Brough S. et al., 2013, *MNRAS*, 435, 2903
 Cameron E., 2011, *PASA*, 28, 128
 Carlberg R. G., Yee H. K. C., Ellingson E., 1997, *ApJ*, 478, 462
 Casteels K. R. V. et al., 2014, *MNRAS*, 445, 1157
 Ching J. H. Y. et al., 2017, *MNRAS*, 469, 4584
 Cid Fernandes R., Stasińska G., Schlickmann M. S., Mateus A., Vale Asari N., Schoenell W., Sodré L., 2010, *MNRAS*, 403, 1036
 Cid Fernandes R., Stasińska G., Mateus A., Vale Asari N., 2011, *MNRAS*, 413, 1687
 Davies L. J. M. et al., 2016, *MNRAS*, 455, 4013
 Davies R. I. et al., 2017, *MNRAS*, 466, 4917
 Davis T. A., Bureau M., 2016, *MNRAS*, 457, 272
 Dolag K., Bartelmann M., Perrotta F., Baccigalupi C., Moscardini L., Meneghetti M., Tormen G., 2004, *A&A*, 416, 853
 Dressler A., Shectman S. A., 1988, *AJ*, 95, 985
 Driver S. P. et al., 2011, *MNRAS*, 413, 971
 Ebeling H., Stephenson L. N., Edge A. C., 2014, *ApJ*, 781, L40
 Ehler S., Allen S. W., Brandt W. N., Xue Y. Q., Luo B., von der Linden A., Mantz A., Morris R. G., 2013, *MNRAS*, 428, 3509
 Einasto M. et al., 2012, *A&A*, 540, A123
 Ellison S. L., Patton D. R., Mendel J. T., Scudder J. M., 2011, *MNRAS*, 418, 2043
 Ellison S. L., Patton D. R., Hickox R. C., 2015, *MNRAS*, 451, 35
 Fabian A. C., 1994, *ARA&A*, 32, 277
 Fraser-McKelvie A., Brown M. J. I., Pimbblet K. A., 2014, *MNRAS*, 444, L63
 Fumagalli M., Fossati M., Hau G. K. T., Gavazzi G., Bower R., Sun M., Boselli A., 2014, *MNRAS*, 445, 4335
 Gavazzi G., Savorgnan G., Fumagalli M., 2011, *A&A*, 534, A31
 Gilmour R., Gray M. E., Almaini O., Best P., Wolf C., Meisenheimer K., Papovich C., Bell E., 2007, *MNRAS*, 380, 1467
 Giovanelli R., Haynes M. P., 1985, *ApJ*, 292, 404
 Gordon Y. A. et al., 2017, *MNRAS*, 465, 2671
 Green T. S. et al., 2016, *MNRAS*, 461, 560
 Grootes M. W. et al., 2017, *AJ*, 153, 111
 Haines C. P. et al., 2012, *ApJ*, 754, 97
 Han J. et al., 2015, *MNRAS*, 446, 1356
 Harcastle M. J., Evans D. A., Croston J. H., 2007, *MNRAS*, 376, 1849
 Hickson P., 1997, *ARA&A*, 35, 357
 Hopkins A. M. et al., 2013, *MNRAS*, 430, 2047
 Kauffmann G. et al., 2003, *MNRAS*, 346, 1055
 Kenney J. D. P., van Gorkom J. H., Vollmer B., 2004, *AJ*, 127, 3361
 Kewley L. J., Dopita M. A., Sutherland R. S., Heisler C. A., Trevena J., 2001, *ApJ*, 556, 121
 Krongold Y., Dultzin-Hacyan D., Marziani P., 2002, *ApJ*, 572, 169
 Liske J. et al., 2015, *MNRAS*, 452, 2087
 Lopes P. A. A., Ribeiro A. L. B., Rembold S. B., 2017, *MNRAS*, 472, 409
 Mahajan S., Raychaudhury S., Pimbblet K. A., 2012, *MNRAS*, 427, 1252
 Marshall M. A., Shabala S. S., Krause M. G. H., Pimbblet K. A., Croton D. J., Owers M. S., 2018, *MNRAS*, 474, 3615
 Martini P., Kelson D. D., Kim E., Mulchaey J. S., Athey A. A., 2006, *ApJ*, 644, 116
 Menon T. K., 1995, *MNRAS*, 274, 845
 Moore B., Katz N., Lake G., Dressler A., Oemler A., 1996, *Nature*, 379, 613
 Munari E., Biviano A., Borgani S., Murante G., Fabjan D., 2013, *MNRAS*, 430, 2638
 Navarro J. F., Frenk C. S., White S. D. M., 1996, *ApJ*, 462, 563
 Oh S. et al., 2014, *ApJ*, 790, 43
 Oman K. A., Hudson M. J., 2016, *MNRAS*, 463, 3083
 Oman K. A., Hudson M. J., Behroozi P. S., 2013, *MNRAS*, 431, 2307
 Ostriker J. P., 1980, *Comments Astrophys.*, 8, 177
 Owers M. S., Couch W. J., Nulsen P. E. J., Randall S. W., 2012, *ApJ*, 750, L23
 Owers M. S. et al., 2013, *ApJ*, 772, 104
 Owers M. S. et al., 2017, *MNRAS*, 468, 1824

- Pentericci L. et al., 2013, *A&A*, 552, A111
Pimblet K. A., Jensen P. C., 2012, *MNRAS*, 426, 1632
Pimblet K. A., Shabala S. S., Haines C. P., Fraser-McKelvie A., Floyd D. J. E., 2013, *MNRAS*, 429, 1827
Pinkney J., Roettiger K., Burns J. O., Bird C. M., 1996, *ApJS*, 104, 1
Poggianti B. M., Wu H., 2000, *ApJ*, 529, 157
Poggianti B. M. et al., 2017, *Nature*, 548, 304
Rines K., Geller M. J., Kurtz M. J., Diaferio A., 2005, *AJ*, 130, 1482
Robotham A. S. G. et al., 2011, *MNRAS*, 416, 2640
Robotham A. S. G. et al., 2014, *MNRAS*, 444, 3986
Rubin V. C., Hunter D. A., Ford W. Kent J., 1991, *ApJS*, 76, 153
Ruderman J. T., Ebeling H., 2005, *ApJ*, 623, L81
Sanchez S. F. et al., 2017, *Rev. Mex. Astron. y Astrofísica*, in press, preprint ([arXiv:1709.05438](https://arxiv.org/abs/1709.05438))
Sanders D. B., Soifer B. T., Elias J. H., Madore B. F., Matthews K., Neugebauer G., Scoville N. Z., 1988, *ApJ*, 325, 74
Schulz S., Struck C., 2001, *MNRAS*, 328, 185
Shen Y., Mulchaey J. S., Raychaudhury S., Rasmussen J., Ponman T. J., 2007, *ApJ*, 654, L115
Shimizu M., Kitayama T., Sasaki S., Suto Y., 2003, *ApJ*, 590, 197
Smith R. J. et al., 2004, *AJ*, 128, 1558
Stasińska G., Cid Fernandes R., Mateus A., Sodré L., Asari N. V., 2006, *MNRAS*, 371, 972
Taylor E. N. et al., 2011, *MNRAS*, 418, 1587
Tonnesen S., Bryan G. L., 2009, *ApJ*, 694, 789
Tzanavaris P. et al., 2014, *ApJS*, 212, 9
Viola M. et al., 2015, *MNRAS*, 452, 3529
Wang T. et al., 2017, *A&A*, 601, A63
Woods D. F., Geller M. J., 2007, *AJ*, 134, 527

This paper has been typeset from a $\text{\TeX}/\text{\LaTeX}$ file prepared by the author.